

Article

Nucleation, Coalescence, and Thin-Film Growth of Triflate-Based Ionic Liquids on ITO, Ag, and Au Surfaces

Mariana S. M. Teixeira, Luís M. N. B. F. Santos  and José C. S. Costa * 

CIQUP, Institute of Molecular Sciences (IMS), Department of Chemistry and Biochemistry, Faculty of Science, University of Porto, Rua do Campo Alegre, P4169-007 Porto, Portugal

* Correspondence: jose.costa@fc.up.pt

Abstract: This study investigates the nucleation and growth of micro-/nanodroplets of triflate-based ionic liquids (ILs) fabricated by vapor deposition on different surfaces: indium tin oxide (ITO); silver (Ag); gold (Au). The ILs studied are constituted by the alkylimidazolium cation and the triflate anion—[C_nC₁im][OTF] series. One of the key issues that determine the potential applications of ILs is the wettability of surfaces. Herein, the wetting behavior was evaluated by changing the cation alkyl chain length (C₂ to C₁₀). A reproducible control of the deposition rate was conducted employing Knudsen cells, and the thin-film morphology was evaluated by high-resolution scanning electron microscopy (SEM). The study reported here for the [C_nC₁im][OTF] series agrees with recent data for the [C_nC₁im][NTf₂] congeners, highlighting the higher wettability of the solid substrates to long-chain alkylimidazolium cations. Compared to [NTf₂], the [OTF] series evidenced an even more pronounced wetting ability on Au and coalescence processes of droplets highly intense on ITO. Higher homogeneity and film cohesion were found for cationic groups associated with larger alkyl side chains. An island growth was observed on both Ag and ITO substrates independently of the cation alkyl chain length. The Ag surface promoted the formation of smaller-size droplets. A quantitative analysis of the number of microdroplets formed on Ag and ITO revealed a trend shift around [C₆C₁im][OTF], emphasizing the effect of the nanostructuration intensification due to the formation of nonpolar continuous domains.



Citation: Teixeira, M.S.M.; Santos, L.M.N.B.F.; Costa, J.C.S. Nucleation, Coalescence, and Thin-Film Growth of Triflate-Based Ionic Liquids on ITO, Ag, and Au Surfaces. *Colloids Interfaces* **2022**, *6*, 46. <https://doi.org/10.3390/colloids6030046>

Received: 8 August 2022

Accepted: 5 September 2022

Published: 7 September 2022

Publisher's Note: MDPI stays neutral with regard to jurisdictional claims in published maps and institutional affiliations.



Copyright: © 2022 by the authors. Licensee MDPI, Basel, Switzerland. This article is an open access article distributed under the terms and conditions of the Creative Commons Attribution (CC BY) license (<https://creativecommons.org/licenses/by/4.0/>).

Keywords: ionic liquids; triflate; imidazolium; physical vapor deposition; thin films; nanodroplets; nucleation; coalescence; Knudsen effusion; SEM; interfacial tension

1. Introduction

Ionic liquids (ILs) are a class of compounds constituted by ionic species that are stable in the liquid phase at a given temperature. ILs are formed from the association of organic cations and organic or inorganic anions and commonly display an asymmetric structure and delocalized electrostatic charges. They exhibit well-organized nanostructures with polar and nonpolar regions that influence their physical–chemical properties [1–5]. ILs have become a hot research subject in multidisciplinary fields such as chemistry, physics, biology, and materials engineering [6–10]. In particular, ILs are used in electrochemical energy applications and are increasingly being studied by researchers who have been exploring their unique properties since they are easily manipulable, and their use involves fewer energy costs when compared to common salts that have higher melting temperatures [11,12]. ILs can be used as low-environmental-impact solvents due to their low vapor pressure promoting sustainability [13–15]. The properties of ILs can be tuned with the combination of different cation–anion pairs. Most ILs share common characteristics such as high ionic conductivity, high viscosity, low vapor pressure at room temperature, chemical and thermal stability, a wide electrochemical range, and a particular wetting behavior [16–20]. The most common low-volatile ILs are constituted by an alkylimidazolium cation [21–23]. The properties of the ILs strongly depend on the size of the alkyl chains associated with the

cationic group and the symmetry [24–28]. The nanostructures of ILs consist of the bonding of nonpolar domains and aliphatic chains, with aromatic groups that form polar domains together with the anions. Depending on the size of the alkyl chain, the nanosegregation between polar and nonpolar domains is highly dependent on the alkyl side chain length: for shorter alkyl chains connected to the polar group, the contribution of the nonpolar domains to the structural organization, because they are small, is less relevant; for larger alkyl chains, both domains have a significant impact on the structural organization of the ionic liquid [2,29]. Different authors showed that for alkyylimidazolium cations, there is a critical alkyl size (CAS) at around C_6 for the asymmetric series $[C_nC_1im]$ —this interesting characteristic of the ILs is verified through extensive studies of their thermophysical properties such as the enthalpy of vaporization [16,26], surface tension [17], and thermal behavior [30,31]. Consistent and accurate measurements of these properties have proved the nanostructural modifications of an ionic liquid at the CAS. The structural modifications were also observed for thin films of bis(trifluoromethylsulfonyl)imide ($[NTf_2]$)-based ILs ($[C_nC_1im][NTf_2]$ series) [32,33]. To progress further, this work aims to investigate the structural/morphological modifications at the microscale for the triflate ($[OTF]$)-based ILs ($[C_nC_1im][OTF]$ series). Thin ionic liquid films consist of multiple monolayers (ML, closed layers of ion pairs with cations and anions on top of each other [34]), and their morphology and structure depend on the nanostructuring of the ILs as well on the film deposition process and the nature of the substrate. Vapor deposition is a very reproducible method for depositing low-volatile ionic liquids [32,33,35–40]. The formation of a thin ionic liquid film starts with the process of nucleation, which is conditioned by a minimum free area to promote nucleation (MFAN) and depends on the strong or weak substrate–ionic liquid interaction [32,35,41–44]. After the formation of stable clusters, the film grows by two main processes: (1) coalescence of native clusters increases the size of stable clusters—the first order of coalescence; (2) coalescence between droplets that had already coalesced—second order of coalescence [35]. The mechanisms of nucleation and growth of thin ionic liquid films also reflect the structural changes due to the varied sizes of the alkyl chains associated with the cation and are observable in the droplets formed after the deposition and on the wettability. The coalescence of clusters on solvophobic surfaces leads to the formation of droplets that have an elevated level of sphericity [33,35], and the analysis of the contact angle is used to evaluate this as well as the affinity of the IL substrate (wettability of the surfaces) [32]. For a macroscopic droplet, Young’s equation ($\gamma_{s-v} = \gamma_{s-l} + \gamma_{l-v} \cos(\theta_c)$) correlates the contact angle (θ_c) with the different interfacial tensions of the system: surface tension of the substrate (γ_{s-v}); surface tension of liquid (γ_{l-v}); substrate–ionic liquid interfacial tension (γ_{s-l}) [45,46]. Young’s equation assumes that the substrates are ideal, i.e., flat, rigid, perfectly smooth, and chemically homogeneous and inert. Furthermore, it assumes that the system is stable (there is no chemical interaction between the liquid and the substrate) and macroscopic. As the presented criteria are difficult to achieve, it is admitted that this contact angle is static, for a simpler and faster approach. The contact angle/wetting behavior also depends on the type of surface roughness, which affects the total surface energy [47–49]. At a nanoscale level, a modified Young’s equation should be considered as detailed elsewhere [50,51]. Contact angles of nanodroplets can be measured from the height profiles obtained through a high-precision atomic force microscopy (AFM) characterization as reported in recent work [32].

The main focus of this work is the wetting behavior of alkyylimidazolium ionic liquids belonging to the $[OTF]$ series (Figure 1) by varying the alkyl chain size of the cation and changing the deposition surface: indium tin oxide (ITO); silver (Ag); gold (Au). It is an innovative study since the morphological study of the $[C_nC_1im][OTF]$ series at micro-/nanoscale, to date, has never been studied in such detail as, for example, the $[NTf_2]$ series [32–40]. This work shows that the size of the alkyl chain highly affects the wetting behavior of the ILs, which was reflected in the film formation and respective morphology, differently on the three surfaces. The morphology, shape, and droplet size distribution were investigated for one coverage: 50 ML. The deposition of each ionic liquid was made

simultaneously onto ITO, Ag, and Au surfaces. A high-resolution scanning electron microscope (SEM) was used to provide detailed images of the micro-/nanodroplets or coalesced films. The overall comparison of SEM images obtained at the same magnification and the analysis of the droplet size distribution provided relevant insights into the different nucleation and coalescence mechanisms of the ionic liquids. An excellent wettability behavior was found on the Au surface, especially for the long-chain ILs that revealed a strong ability for the formation of a homogenous and compact coalesced film. ITO and Ag surfaces were found to be more solvophobic surfaces to the ILs as indicated by the preferential 3D growth (island growth) exhibited for all the ILs on these surfaces. The Ag surface exhibited a lower MFAN (larger number of micro/nanodroplets formed) and better wettability for ionic liquids with a larger alkyl chain compared to the ITO surface. The morphological analysis showed substantial changes between short- and long-chain ILs. A trend shift around C6 (CAS) was observed. The differences in the wetting behavior are truly relevant for the applications of ILs. In particular, controlling the wettability of solid surfaces to the ILs is relevant for the development of materials with good interface-controlled behavior. The wetting properties of ILs are of relevant interest for many applications such as sensors, electrochemical devices, lubrication, separation technologies, and catalysis, among others [10–20].

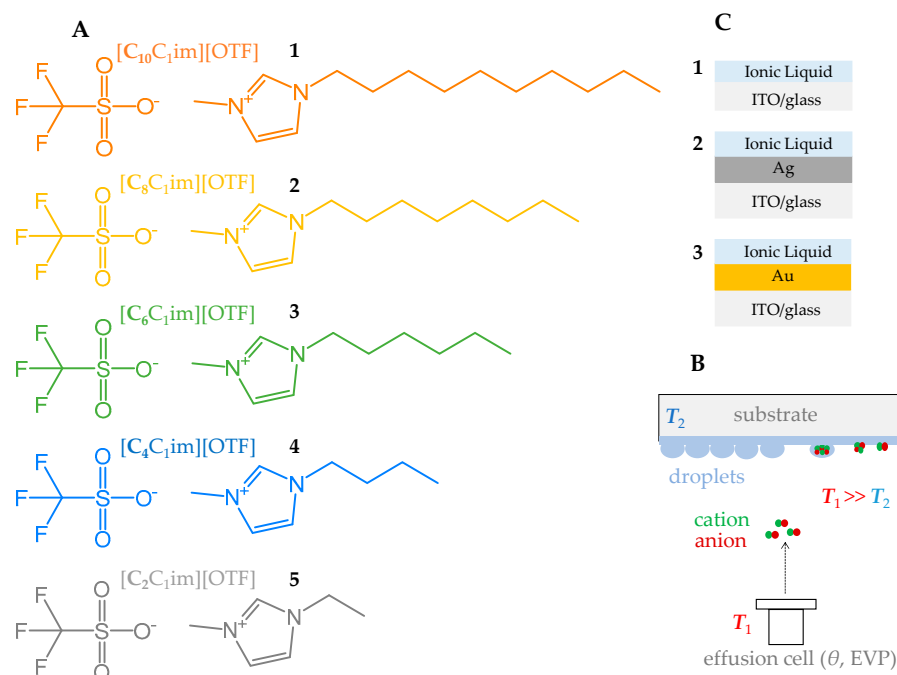


Figure 1. Molecular structure of the studied triflate-based ionic liquids and the adopted acronyms (A): 1-decyl-3-methylimidazolium triflate, $[C_{10}C_1im][OTF]$; 1-octyl-3-methylimidazolium triflate, $[C_8C_1im][OTF]$; 1-hexyl-3-methylimidazolium triflate, $[C_6C_1im][OTF]$; 1-butyl-3-methylimidazolium triflate, $[C_4C_1im][OTF]$; 1-ethyl-3-methylimidazolium triflate, $[C_2C_1im][OTF]$. Schematic representation of the effusion process (T_1 and T_2 denote the evaporation temperature and the substrate temperature, respectively) of the ionic liquids from the Knudsen cell (B). Scheme of the thin-film architectures fabricated (C): substrate ITO/glass coated with ionic liquid (1); substrate Ag/ITO/glass coated with ionic liquid (2); substrate Au/ITO/glass coated with ionic liquid (3).

2. Materials and Methods

Five different ILs were studied to evaluate the behavior of the $[C_nC_1im][OTF]$ series with the change in length of one of the alkyl chains. The following ILs were purchased from Iolitec, with a state of purity of >99%, and used in this work: 1-ethyl-3-methylimidazolium triflate, $[C_2C_1im][OTF]$; 1-butyl-3-methylimidazolium triflate, $[C_4C_1im][OTF]$; 1-hexyl-3-methylimidazolium triflate, $[C_6C_1im][OTF]$; 1-octyl-3-methylimidazolium triflate,

[C₈C₁im][OTF]; 1-decyl-3-methylimidazolium triflate, [C₁₀C₁im][OTF]. The volatile content of the ILs was removed by low-pressure ($p < 0.1$ Pa) thermal evaporation at $T = 423$ K. Figure 1 depicts the molecular structure of the cation–anion pairs and schematizes the effusion process of the ILs from the Knudsen cell and the thin film architectures fabricated.

Each ionic liquid was deposited onto surfaces of indium tin oxide (ITO)/glass, silver (Ag)/ITO/glass, and gold(Au)/ITO/glass substrates. The glass substrates (10 mm × 10 mm × 1.1 mm) coated with a thin film of ITO (180 nm of thickness) were commercially purchased from the Praezisions Glas & Optik GmbH company. These substrates were cleaned with high-purity ethanol in an ultrasonic bath and dried with ultra-high purity grade argon (>99.99%). The metallic films (Ag and Au) were deposited onto the ITO-coated glass substrates by DC magnetron sputtering through the Cressington 108 Auto Sputter Coater instrument. Argon plasma was used, and the sputtering process was accomplished by using a discharge current of 40 mA. High-purity (>99.9%) Ag and Au targets were employed. The metallic films were fabricated with an approximate thickness of 100 nm. Immediately after the deposition of the metallic films, both substrates (ITO, Ag/ITO, and Au/ITO) were introduced into a clean vacuum system for the deposition of ILs. Most samples exposed to the atmosphere are subjected to carbon contamination. Theoretically, metallic films are expected to be less covered with a nanolayer of carbon than ITO/glass surfaces. We always tried to minimize the time of air exposure to prevent significant contamination with adventitious carbon. The substrates were quickly introduced into the vacuum chamber, which was degassed at 10^{-4} Pa. Low contamination levels of carbon for samples exposed to air for less than 2 min have been demonstrated in another study [52].

Ionic liquids films were fabricated with 50 ML of thickness. The height (h) of one ML can be estimated as $(h = M/(N_A \times \rho))^{1/3}$, where M is the molar mass, ρ is the density, and N_A is Avogadro's constant: $h = 6.77$ Å, $h = 7.16$ Å, $h = 7.51$ Å, $h = 7.81$ Å, and $h = 8.13$ Å correspond to 1 ML of [C₂C₁im][OTF], [C₄C₁im][OTF], [C₆C₁im][OTF], [C₈C₁im][OTF], and [C₁₀C₁im][OTF], respectively. For the formation of thin ionic liquid films, a customized procedure of physical vapor deposition (PVD) based on the Knudsen effusion method, was used—the ThinFilmVD apparatus (details presented in Figures S1–S3) [53]. This PVD system provides a film deposition under very reduced pressure ($p < 10^{-4}$ Pa). A strong vacuum facilitates the movement of the vapor particles directly reaching the substrate where these vapors again change to a condensed state, thus forming a thin layer. The use of Knudsen effusion cells allows very precise control of the mass flow rate. This method is highly reproducible, and the films formed are very well-defined and with a rigorously known thickness [32,35,53–56]. Thermal evaporation occurs by placing the ionic liquid in an effusion cell (Knudsen cell) designed to maintain the substance in equilibrium under accurate and reproducible temperatures. The dependence of vapor pressure with temperature is used to derive the mass flow rate effused directly from the Knudsen cell orifice. The reproducibility and control of this method for the vacuum thermal evaporation of ILs were detailed and reported in previous work [56].

For the evaluation and control of the film thickness, a quartz crystal microbalance (QCM), Inficon model STM-2, was used. For this method, the mass flow rate, ϕ , is obtained according to a derived form of the Knudsen equation, Equation (1): $\phi_{\text{substrate}}$ and $\phi_{\text{Knudsen cell}}$ represent the mass flow rates, g is a geometric factor dependent on the Knudsen cell-substrate distance, T represents the evaporation temperature, p the equilibrium vapor pressure, w_o the transmission probability factor, M the molar mass of the effused vapor, m the mass of the vapor, t the effusion time, and A_o the area of the Knudsen cell orifice [16,26,32,33,35,36,53–56].

$$\phi_{\text{substrate}} = g \cdot \phi_{\text{Knudsen cell}} = g \cdot \frac{p \cdot w_o \cdot \sqrt{M}}{\sqrt{2\pi RT}} = g \cdot \frac{m}{A_o \cdot t} \quad (1)$$

[C₂C₁im][OTF], [C₄C₁im][OTF], [C₆C₁im][OTF], [C₈C₁im][OTF], and [C₁₀C₁im][OTF] were deposited under similar experimental conditions: thickness of 50 ML; each deposition

simultaneously performed on ITO, Ag, and Au surfaces—maintained at a constant temperature of $T = (283.2 \pm 0.2)$ K; deposition rate of $\phi_{\text{substrate}} = (0.20 \pm 0.05)$ Å/s. $[\text{C}_2\text{C}_1\text{im}][\text{OTF}]$, $[\text{C}_4\text{C}_1\text{im}][\text{OTF}]$, and $[\text{C}_6\text{C}_1\text{im}][\text{OTF}]$ were evaporated at $T = (513.2 \pm 0.1)$ K whereas $[\text{C}_8\text{C}_1\text{im}][\text{OTF}]$ and $[\text{C}_{10}\text{C}_1\text{im}][\text{OTF}]$ were evaporated at $T = (523.2 \pm 0.1)$ K. For each experiment, the effusion time was monitored to achieve the desired 50 ML of film thickness. More details are presented in Table S1. The time of air exposure of the substrates and the ionic liquid films was always minimized in order to prevent substantial contamination. The films were stored under an argon atmosphere, and SEM characterization was carried out ≈ 1 week after film deposition. Most of the data and conclusions of this work are made at the microscale, and low levels of carbon contamination do not have a strong impact on the film morphologies reported. Nonetheless, the presence of adventitious carbon surface contamination should be considered and could have an additional influence on the phenomena observed at a nanoscale level [52,57]. In this case, the conclusions drawn from the experiments must be taken with some care.

For the morphological characterization of the samples, a high-resolution scanning electron microscope (SEM, FEI Quanta 400 FEG ESEM instrument) was used. Topographic images of the micro-/nanodroplets or coalesced films of the ILs deposited on the different solid surfaces were obtained at different magnifications. Micrographs were acquired using two detectors: a backscattered electron detector (BSE) and a secondary electron detector (SE). The accelerating voltage was 10 kV, and the detector was placed at a working distance of 10 mm. Magnifications of $500\times$, $2000\times$, and $5000\times$ were used to obtain the images. The shape, surface coverage, and size distribution of the micro-/nanodroplets observed in the SEM images were analyzed with *ImageJ* software [58].

3. Results

A detailed morphological analysis of the SEM images was used to evaluate the nucleation and growth tendency of the five different ILs at a microscale level. The typical processes of nucleation and growth of ILs are schematized in Figure S4. The experimental results were further analyzed by image processing with *ImageJ* software, which allowed us to obtain the droplet size distribution and respective surface coverage of the micro-/nanodroplets formed. Figures 2–4 show the morphology of the different ILs (50 ML) deposited under the same experimental conditions on the three solid surfaces: ITO/glass; Ag/ITO/glass; Au/ITO/glass. SEM images of the surfaces are presented in Figure S5. The topography of the surfaces appeared to be quite similar, suggesting that the roughness factor did not significantly influence the results obtained. The high-magnification images (on the left of each figure) were acquired by secondary electron imaging and provided details on the three-dimensional appearance of the droplets. SEM micrographs acquired by backscattered electron imaging (low magnification SEM image on the center of each figure) were used to characterize a large area of the film surface and, hence, they are more representative of the system under study. The histograms displaying the droplet distribution were obtained by image processing from those micrographs (on the right of each figure). There were no significant changes in the droplet size distribution depending on the time after ionic liquid deposition. In fact, the microdroplets formed by thermal evaporation of ILs constituted by an alkylimidazolium cation and the [OTF] or [NTF₂] anions were very stable, and no coalescence effects occurred without the use of surface treatments with energetic particles [33]. Wetting behavior studies of ILs at macroscopic and mesoscopic scales revealed a reduced impact of heat exposure on the morphology of the ionic liquid droplets [32]. On the other hand, time-dependent changes in the adsorption/desorption of the ILs on metal surfaces have been reported to a few layers deposited on the substrate [59].

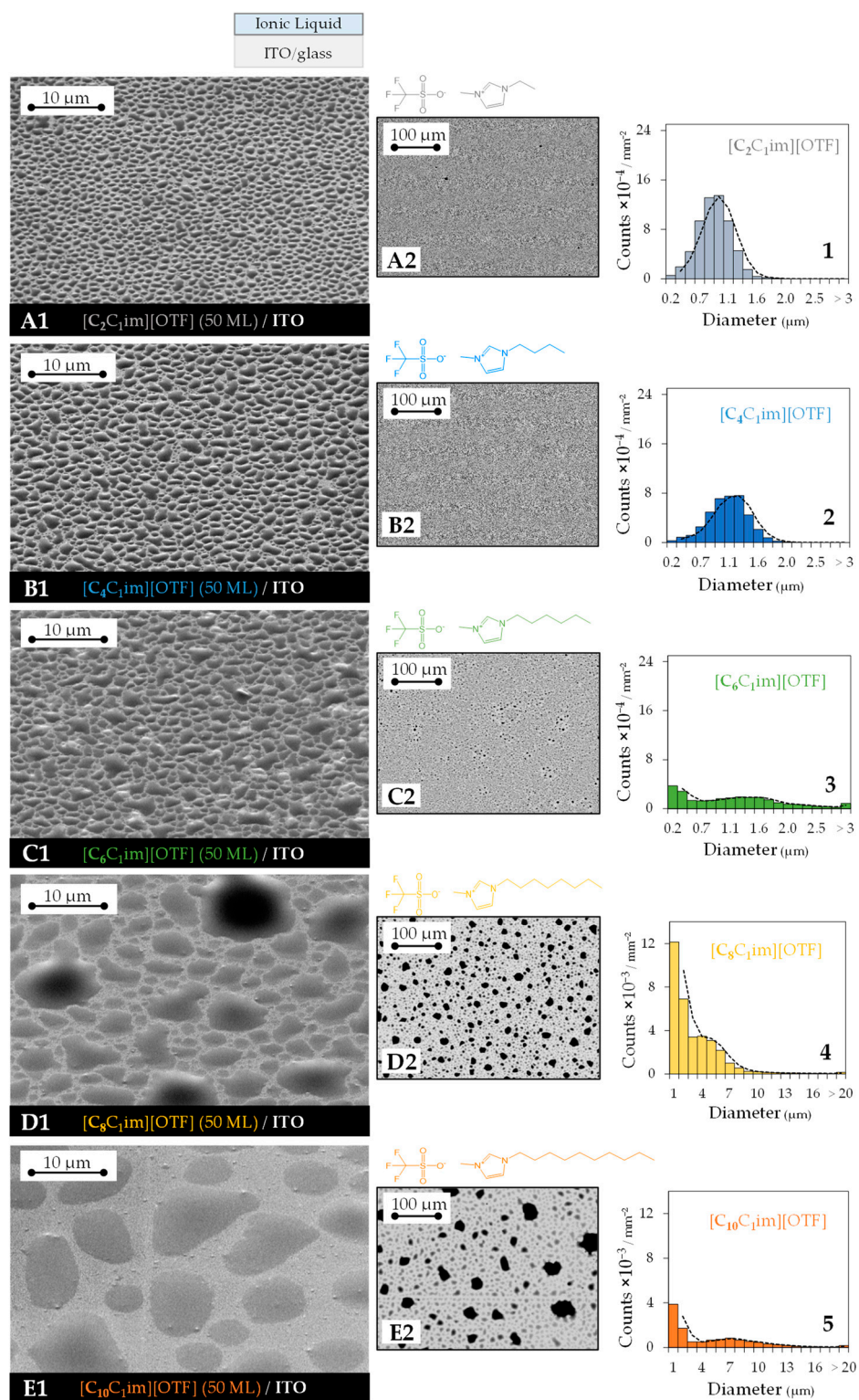


Figure 2. Micrographs acquired through high-resolution scanning electron microscopy of thin ionic liquid films (50 monolayers, ML) of $[\text{C}_2\text{C}_1\text{im}][\text{OTF}]$ (A1,A2), $[\text{C}_4\text{C}_1\text{im}][\text{OTF}]$ (B1,B2), $[\text{C}_6\text{C}_1\text{im}][\text{OTF}]$ (C1,C2), $[\text{C}_8\text{C}_1\text{im}][\text{OTF}]$ (D1,D2), and $[\text{C}_{10}\text{C}_1\text{im}][\text{OTF}]$ (E1,E2) deposited onto surfaces of ITO/glass. Lateral views at 45° (magnification of $5000\times$) obtained by secondary electron imaging (A1–E1) and top views (magnification of $500\times$) obtained by backscattered electron imaging (A2–E2). The histograms (inserts 1, 2, 3, 4 and 5) present the droplet’s size distribution for each sample.

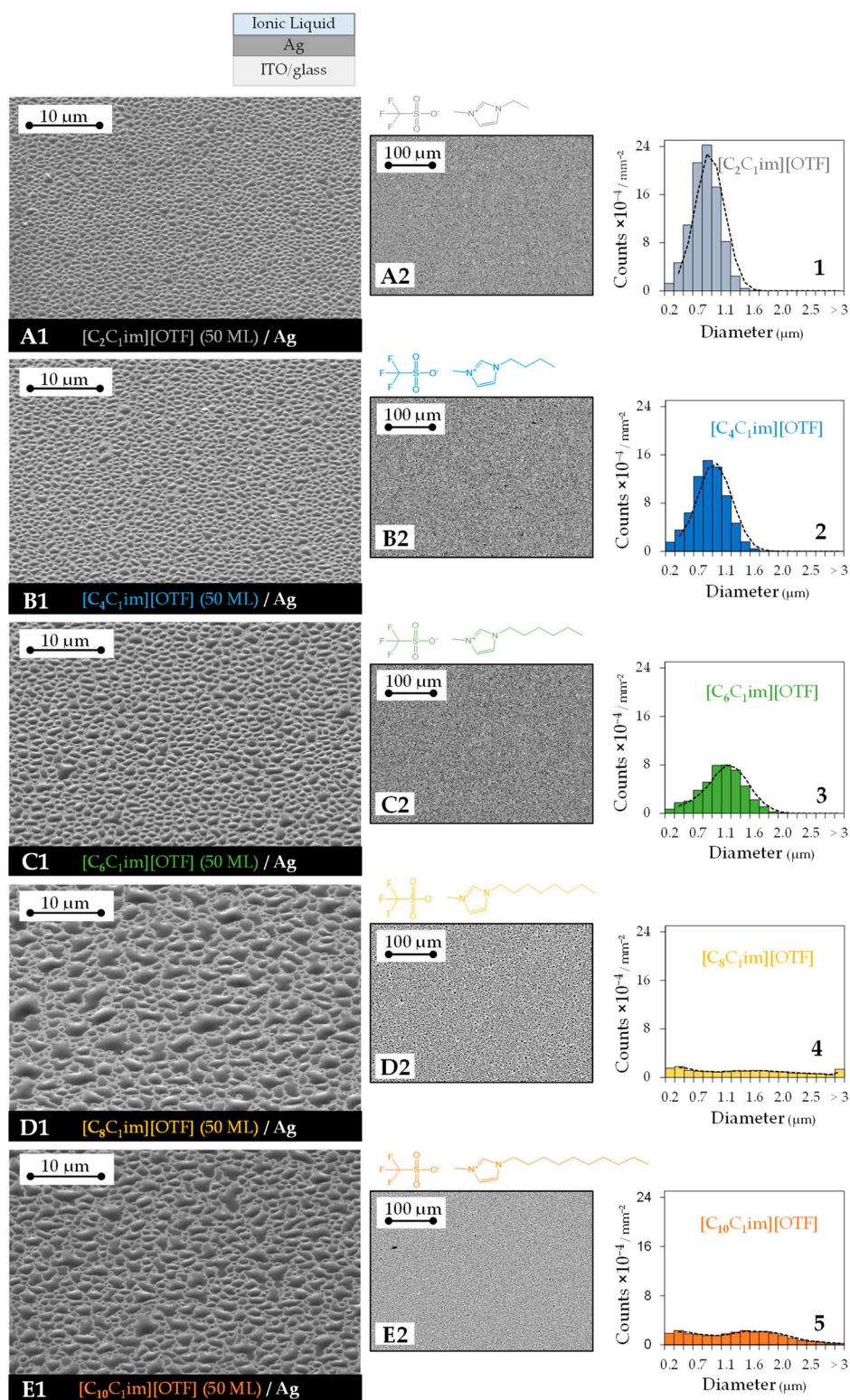


Figure 3. Micrographs acquired through high-resolution scanning electron microscopy of thin ionic liquid films (50 monolayers, ML) of [C₂C₁im][OTF] (A1,A2), [C₄C₁im][OTF] (B1,B2), [C₆C₁im][OTF] (C1,C2), [C₈C₁im][OTF] (D1,D2), and [C₁₀C₁im][OTF] (E1,E2) deposited onto surfaces of Ag/ITO/glass. Lateral views at 45° (magnification of 5000×) obtained by secondary electron imaging (A1–E1) and top views (magnification of 500×) obtained by backscattered electron imaging (A2–E2). The histograms (inserts 1, 2, 3, 4 and 5) present the droplet's size distribution for each sample.

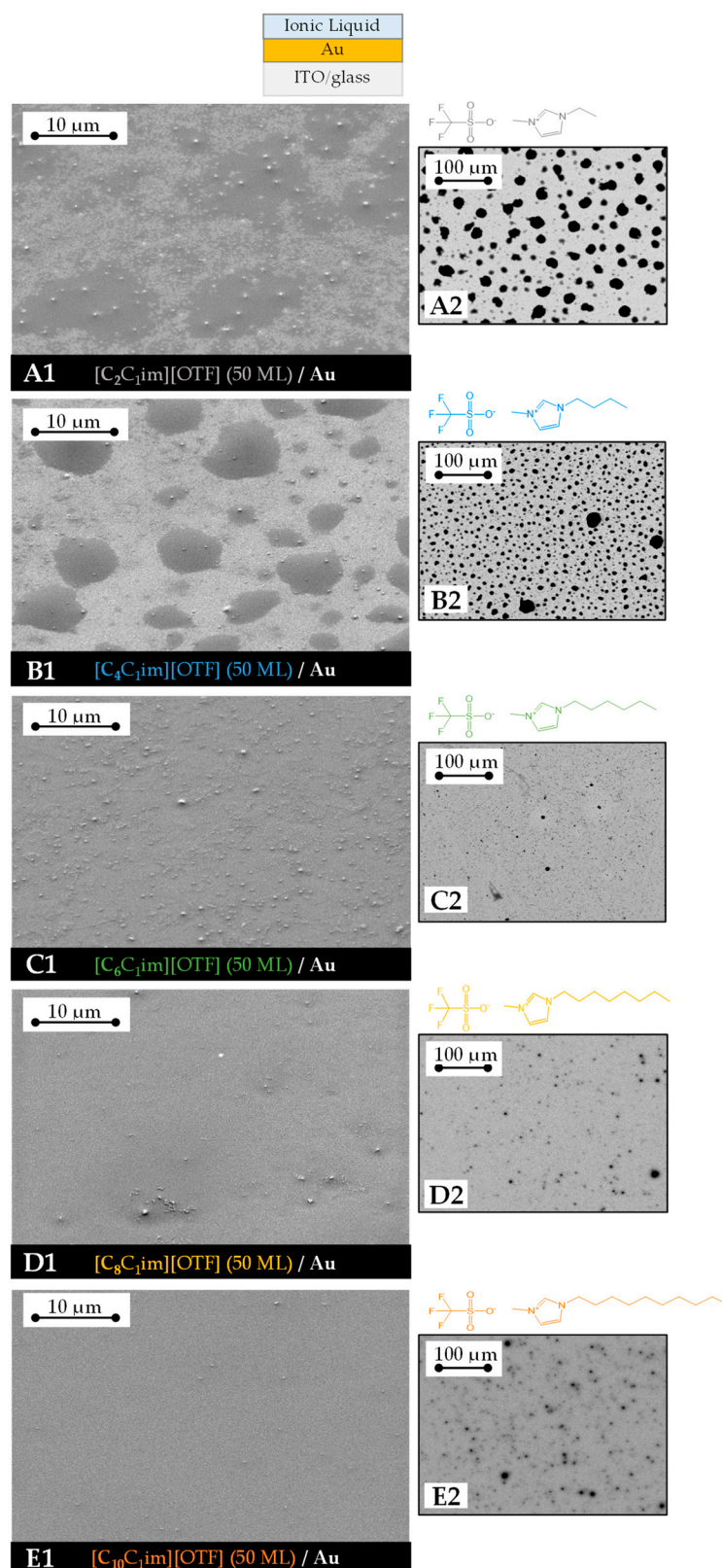


Figure 4. Micrographs acquired through high-resolution scanning electron microscopy of thin ionic liquid films (50 monolayers, ML) of [C₂C₁im][OTF] (A1,A2), [C₄C₁im][OTF] (B1,B2), [C₆C₁im][OTF] (C1,C2), [C₈C₁im][OTF] (D1,D2), and [C₁₀C₁im][OTF] (E1,E2) deposited onto surfaces of Au/ITO/glass. Lateral views at 45° (magnification of 5000×) obtained by secondary electron imaging (A1–E1) and top views (magnification of 500×) obtained by backscattered electron imaging (A2–E2).

In general, through direct analysis of the SEM micrographs, there was a formation of micro-/nanodroplets on Ag and ITO surfaces whereas the Au surfaces promoted a formation of coalesced films of ILs. In addition, on both ITO and Ag surfaces, the size and distribution of micro-/nanodroplets were clearly dependent on the length of the alkyl chain: an increase in the cation alkyl chain reflects a larger size of the droplets formed.

On the ITO surface (Figure 2), an increase in the non-polar domains of the ionic liquid (increasing the cation alkyl side chain length) led to strong morphological differentiations in the size, shape, and number of droplets formed. For [C₂C₁im][OTF], the predominant diameter size was between 0.8 and 1.0 μm (graph 1); for [C₄C₁im][OTF], between 1.0 and 1.3 μm (graph 2); and for [C₆C₁im][OTF] (graph 3), between 1.2 and 1.6 μm. For these ILs, there were no visible droplets with diameters greater than 4 μm. A more noticeable differentiation in the droplet size was observed for [C₈C₁im][OTF] (graph 4) and [C₁₀C₁im][OTF] (graph 5) since very large droplets, whose diameter exceeded 20 μm, were formed (Figure 2D,E). For both samples, no predominant droplet size was observed. However, there was an increase in the intermediate sizes and the formation of various small droplets. These results may denote that the processes of coalescence are more significant for ILs with larger non-polar domains because the most frequent droplet size increases. When coalescence was intense, as in the cases of [C₈C₁im] and [C₁₀C₁im], there was a formation of many nanodroplets since empty spaces were left exposed. Nevertheless, the more intense coalescence mechanisms for imidazolium-based ILs comprising long alkyl side chains did not lead to a much better wettability: surface coverages of 34 ± 1, 35 ± 2, 39 ± 1, 41 ± 1, and 40 ± 2% were obtained for 50 ML of [C₂C₁im][OTF], [C₄C₁im][OTF], [C₆C₁im][OTF], [C₈C₁im][OTF], and [C₁₀C₁im][OTF], respectively. For the ITO surface, we can also conclude that the increase in the alkyl chain changed the morphology of the droplets on the surface—the droplets become larger and more irregular. These morphological characteristics may be explained by intense processes of coalescence. The irregularity was more evident in the [C₁₀C₁im][OTF] sample, where the droplets were much larger and seemed to have smaller contact angles (Figure 2E1). Despite having an apparent smaller contact angle, the ionic liquid film still did not cover most of the surface area. Although having a lower surface tension, a characteristic of the long-chain alkylimidazolium-based ILs [17], the interfacial tension of ITO-ionic liquid might still be high enough to not allow a complete wetting of the IL, i.e., the wettability remained poor. Although the ITO surfaces had a weak wettability to the films studied, the ionic liquid droplets might be well adsorbed to the surface, highlighting the existence of some ionic liquid–substrate interaction. On the other hand, some irregular shapes of the droplets might be affected by the surface topology of the ITO substrate. Preferential nucleation at the step edges of the ITO surface should be considered as it could have some impact on the droplet morphology/shape [60].

For the Ag surface (Figure 3), two conclusions can be drawn: the number of droplets formed was much higher and the droplets were smaller although they occupied a larger percentage area of the substrate, i.e., higher surface coverage, compared to the ITO. The five different ILs, on the Ag surface, when compared to the ITO, formed droplets with approximate sizes (small and intermediate); therefore, the MFAN may be lower for Ag than for the ITO. This observation can be derived through the higher number of counts when compared to the ITO surface. The total number of counts/mm² on the Ag surface was found to be 1.54, 1.73, and 1.74 times higher than that observed for the ITO surface for [C₂C₁im][OTF], [C₄C₁im][OTF], and [C₆C₁im][OTF], respectively. The Ag surface seems to be a more favorable substrate for the nucleation process, which translates into a better wettability for the imidazolium-based ILs [32], and the coalescence processes of native droplets were delayed on this surface. The surface coverages for 50 ML of ionic liquid deposited onto Ag were 39 ± 1, 37 ± 2, 37 ± 1, 47 ± 2, and 45 ± 4% for [C₂C₁im][OTF], [C₄C₁im][OTF], [C₆C₁im][OTF], [C₈C₁im][OTF], and [C₁₀C₁im][OTF], respectively. The droplets occupied a larger surface area in comparison to the ITO. For [C₂C₁im][OTF], the predominant diameter size was between 0.7 and 0.9 μm (graph 1); for [C₄C₁im][OTF], between 0.8 and 1.0 μm (graph 2); and for [C₆C₁im][OTF], between 1.0 and 1.3 μm (graph 3).

For $[C_8C_1im][OTF]$, the droplets started to have an intermediate size–great size distribution (graph 4) and for $[C_{10}C_1im][OTF]$, there was no significant differentiation in the droplet count for diameters up to 2 μm (graph 5). Droplets with diameters greater than 4 μm were not formed for any of the ILs deposited on the Ag surface. Hence, for this substrate, the increasing size of the alkyl chain did not change, significantly, the morphology of the droplets on the surface (smaller-sized droplets) was highly circular. This change in the circularity of the droplets may indicate that the second-order coalescence mechanisms, on this surface were not as intense as those on the ITO surface.

For the Au surface (Figure 4), all the ILs spread very well, forming isolated droplets with a large size and small contact angle; a significant percentage of the substrate area was filled with the ionic liquid or a fully coalesced thin film. For these samples, secondary electron imaging was especially useful for the inspection of the topography of the sample's surface, allowing us to infer the tridimensional appearance of the films/droplets. For instance, Figure 4A1 displays ionic liquid droplets with a reduced contact angle; this is not visible by looking at the corresponding backscattered electron image (Figure 4A2). There were almost no small droplets around the bigger ones because of the coalescence, which also contributed to good wettability (droplets with lower height and higher width). For $[C_2C_1im][OTF]$ and $[C_4C_1im][OTF]$, there was a preferential formation of 3D droplets as clearly evidenced by Figure 4A,B, whereas $[C_6C_1im][OTF]$ (Figure 4C), $[C_8C_1im][OTF]$ (Figure 4D), and $[C_{10}C_1im][OTF]$ (Figure 4E) exhibited a very smooth morphology, highlighting the formation of a highly cohesive coalesced film. The PVD process of ILs on Au surfaces could lead to the formation of nanodroplets with low contact angles (<10 degrees) and high proximity, i.e., very low MFAN [32]. The droplets might be more spread out due to the low interfacial tension or good affinity between the IL and the substrate. Independently of the anion type ([OTF] or [NTf₂]), the imidazolium-based ILs exhibited an excellent affinity for the Au surface. The formation of 3D droplets for the short-chain ionic liquids might be derived from the higher surface tension of these ILs. For ILs formed by a long alkyl chain associated with the imidazolium cation, both ionic liquid/vapor and ionic liquid/Au interfacial tensions could be lower [17,32]. These characteristics could induce a formation of a film with a low contact angle and, hence, the wettability of the Au substrate to the thin ionic liquid film was even more improved. Additional details on the morphological characterization of the thin ionic liquid films can be found in Figures S6–S11.

4. Discussion

The wetting behavior at the microscale of ILs belonging to the $[C_nC_1im][OTF]$ series agrees with the achievements recently reported for the $[C_nC_nim][NTf_2]$ series [32], revealing the higher contribution of the substrate nature as well as the imidazolium alkyl side chain length, rather than the [NTf₂] or [OTF] anions, for the wettability of solid surfaces (ITO/glass, and metallic substrates) to the ILs.

Considering the ITO surface, for both [OTF] and [NTf₂] series, the increase in the alkyl side chain length contributes to the formation of larger-size droplets. A more significant droplet coalescence mechanism does not lead to the formation of coalesced films for any of the ILs deposited by PVD. The coalescence of droplets, with special emphasis on the second-order mechanisms, might be more intense for the [OTF]-series as indicated by the film heterogeneity, low circularity, and larger size of the droplets formed for the long-chain alkylimidazolium triflate ILs. Glass and ITO substrates are more solvophobic than metal surfaces to the imidazolium-based ionic liquids [32,33,35,36,61–65]. On these surfaces, the island growth could usually be preferred to 2D independently of the length of the alkyl chain associated with the cationic group. The deposition of ILs by PVD onto ITO/glass substrates usually generates a film with low surface coverage constituted by microdroplets with a contact angle of ≈ 20 degrees [32,33,35]. On the Ag surface, the vacuum thermal evaporation of the [OTF]-based ILs produced a film with a higher total droplet count combined with smaller droplet size. This morphological differentiation of the ionic liquid

droplets formed simultaneously on the ITO and Ag surfaces was also reported for the [NTf₂] series [32]. This work emphasizes that independently of the anion nature, Ag might be a more favorable substrate, rather than ITO, for the nucleation process of the ILs and a more homogeneous droplet size distribution along the entire surface. In addition, contrary to that observed for the ITO surface, the increase in the cation alkyl side chain length led to a higher surface coverage of the droplets/better wettability. For the first ML deposited (on the molecular scale), it is well established that the imidazolium cations lie parallel to the metal surfaces in a highly ordered adsorption geometry [65–67]. This behavior could contribute to the lower MFAN observed. The higher MFAN observed for ITO/glass surfaces could arise from weak adsorption and the consequent high mobility of cation–anion pairs and small clusters. For the long-chain alkylimidazolium-ILs, some authors reported that the alkyl moieties also lie flat on the Ag surface, thus maximizing the interaction with the metallic surface [64]. Overall, a better affinity of Ag to the ILs may be expressed by a low MFAN and less intense mechanisms of coalescence between 3D droplets.

The wettability of Au surfaces to the [C_nC₁im][OTF]-based ILs is also similar to that observed for the [NTf₂]-congeners. Large droplets with reduced contact angles are formed when the ionic liquid is more polar ($n < 6$) [32] and a compact, more homogeneous, and coalesced nanofilm was observed for the ILs constituted by large non-polar domains ($n > 6$). The low interfacial tension of ionic liquid/Au may result from the excellent adsorption efficiency of the cation–anion pairs on Au, including the alkyl chains, as proved by many authors [65–73]. The cation–anion pairs are considered to interact with the Au surface through the formation of image dipoles [73]. The MFAN of the ILs on Au surfaces is even more reduced due to the characteristics of the deposition/effusion process—the ion pairs are homogeneously deposited onto the entire surface—a coalesced film is easily formed, even for small thicknesses (50 ML). The nucleation and growth mechanisms of imidazolium triflate ILs on Au seem to follow the 2D mode with special emphasis on the long-chain alkylimidazolium-based ILs since the long-alkyl chains attached to the Au surface could favor the dispersive interactions with the subsequent alkyl chains deposited. An increase in the film thickness corroborates a tendency for island growth for the more polar ILs.

These results emphasize that the surface where the ILs are thermally evaporated has the greatest influence on the wetting behavior at the microscale. Overall, the Au surfaces have excellent wettability for the ILs as proved by the formation of a thin film with a negligible contact angle due to a reduced solid–liquid interfacial tension. A comparison of the interfacial tension of the ILs with the substrates used should be made with some care since there is a possibility of the formation of a closed wetting layer of ionic liquid (undetectable by SEM) on metal oxides and metals. An example was shown by Rietzler et al. for [C₂C₁im][OTF] [34]. The formation of a closed wetting layer on metal surfaces was reported for various imidazolium-based ILs comprising [NTf₂] or [PF₆] anions [65]. The growth of the ionic liquid film on top of the wetting layer may depend on the nature of the cation–anion pairs and the substrates, as demonstrated in this work for the triflate-based ILs.

For a deeper evaluation of the impact of the length of the cation alkyl side chain on the nucleation and growth of ionic liquid droplets formed on both ITO and Ag surfaces, Figure 5 shows a graphical representation correlating the total number of ionic liquid microdroplets formed as a function of the cation alkyl chain length in the [C_nC₁im][OTF] series. To infer the coalescence trend of each ionic liquid, these representations quantify the number of droplets with a diameter greater than 1 μm.

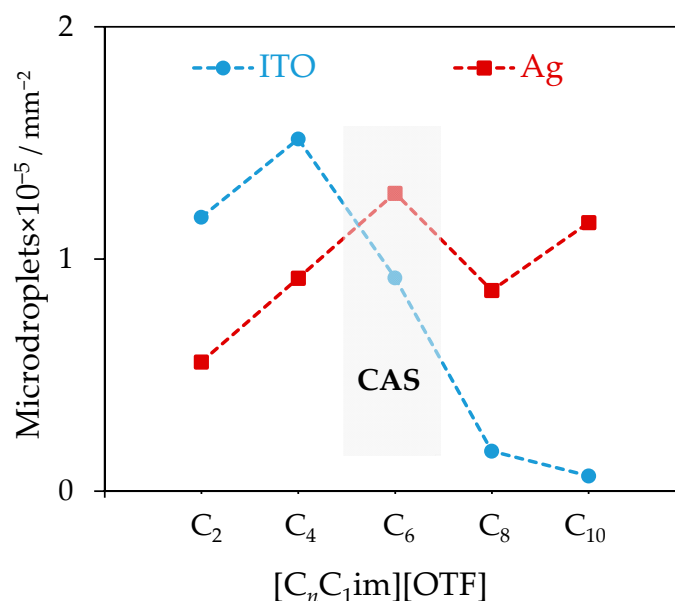


Figure 5. Schematic representation of the number of ionic liquid microdroplets (diameter greater than 1 μm) formed per mm^2 of surface area (ITO—blue circles, Ag—red squares) as a function of each ionic liquid in the $[\text{C}_n\text{C}_1\text{im}][\text{OTF}]$ series.

Through the observation of the trends for both surfaces, there is a clear shift in the behavior around C₆, the CAS. The same shift is also perceived from the dependence of the surface coverage of the microdroplets with the cation alkyl chain length (details are presented in Figure S12). The results/trends for the $[\text{C}_n\text{C}_1\text{im}][\text{OTF}]$ series, quantified in this work, are very similar to those already published by our group for the $[\text{C}_n\text{C}_1\text{im}][\text{NTf}_2]$ series [33]. A trend shift at C₆ may be related to the well-known nanostructural differentiation of alkylimidazolium-based ILs [2]. The effect of the alkyl chain length (trend shift at the CAS) is especially visible for the Ag surface since due to a lower MFAN, the droplet coalescence processes could slow down, which allows us a better observation of this trend change. In general, on ITO, the behavior of the ILs with smaller alkyl chains is similar for both [OTF] and [NTf₂] families. The number of microdroplets increased from C₂ to C₆. Curiously, if all the droplet counts exhibited by the histograms were considered (from 0.2 μm of diameter), an inverse relation would be obtained—a decrease in the number of droplets by increasing the length of the alkyl chains, since the formation of larger droplets presupposes the coalescence of numerous small ones reducing their number. The long-chain ILs of the [OTF] series might have a complex nanostructural organization on the ITO surface. There is a greater differentiation of the coalescence behavior of the droplets formed on the ITO and Ag surfaces. The clear decrease in the number of microdroplets is a result of intense second-order coalescence mechanisms resulting in the formation of large droplets. These mechanisms are particularly highly noticeable for $[\text{C}_{10}\text{C}_1\text{im}][\text{OTF}]$. Due to a weak affinity/interaction ionic liquid-ITO, the ionic liquids deposited could have great mobility on the surface, which makes the coalescence mechanisms very intense—the different droplets tend to merge to be more stable, resulting in poor wettability. For the Ag surface, the ionic liquid might have a greater affinity, which decreases the mobility, delaying this mechanism—the first-order coalesced droplets are well adsorbed to the substrate and do not have enough mobility to produce second-order coalesced droplets. On the Au surface, there is not only the formation of isolated droplets but there is also the formation of a coalesced film (with all ionic liquids) and the formation of agglomerates of ionic liquid, which tend to decrease in size until a coalesced and homogeneous film is formed (this happens as the alkyl chain of the ionic liquid increases). The Au surface revealed an excellent affinity to the long-chain ILs, resulting in excellent wettability. The nanodroplets exhibit very low contact angles and high proximity. The first- and second-order coalescence processes

could occur faster, and a coalesced film formed easily. The experimental trends obtained are related to the structure of the ILs at a molecular level. Nanometer-scale structuring for different classes of ILs has been observed by several authors by using experimental and theoretical models [2,16,20,29]. The nucleation process of ionic liquid clusters may be conditioned by the surface diffusion of the cation–anion pairs on the surface. Both nucleation and coalescence processes are strongly dependent on the relative volumes occupied by the polar and non-polar moieties (alkyl chains) of the ILs. For small alkyl chains, the nonpolar domains are characterized as isolated islands in a continuous polar domain. These nonpolar domains start to coalesce when the alkyl chain length is increased [2,29]. This fundamental description may explain the formation of the first ML of the thin ionic liquid films and supports the experimental data obtained, showing an increase in the number of microdroplets formed from C_2 to C_6 . The successive coalescence of the nonpolar domains leads to the creation of a bicontinuous fluid phase. This structural modification occurs at the CAS and might emphasize the effect of the nanostructuring intensification due to the formation of nonpolar continuous domains.

5. Conclusions

This work contributed to the knowledge of the wetting behavior at the microscale of different ionic liquids (ILs) composed of the triflate anion ([OTF]) and an alkyimidazolium cation ($[C_nC_1im]$) when deposited by vapor deposition onto different solid substrates. The morphological differentiation between short-chain or long-chain alkyimidazolium-based ILs was investigated, for the first time, for an extended $[C_nC_1im][OTF]$ series. The analysis of the droplet size distribution was used to derive important insights into the different nucleation and growth mechanisms of the ILs. The results showed that the wetting behavior on three different surfaces—ITO, Ag/ITO, and Au/ITO—of imidazolium-based ILs, is strongly influenced by the length of the cation alkyl chain. On both Ag and ITO surfaces, the ILs did not form a coalesced thin film, in any of the studied cases, under the established conditions, unlike for the surface of Au. On the Au surface, it was visible that the formation of a thin film with only 50 ML of ionic liquid deposited, especially for the ILs with larger nonpolar domains, for which a very compact, cohesive, and homogenous film was formed. This experimental observation reveals an excellent wetting behavior that might be derived from a low interfacial tension substrate-IL, the low contact angle of the films, and large surface coverage, highlighting a great affinity between the Au surface and the ILs. On the Ag surface, with 50 ML of ionic liquid deposited, the results showed the formation of a higher number of droplets with a large surface coverage in comparison to the ITO. The most frequent droplet sizes of the ILs were lower for the Ag substrate, which indicates that the Ag surface may promote a lower MFAN for the ILs. The similarity of the results obtained in this work for the $[C_nC_1im][OTF]$ series with those reported for the $[C_nC_1im][NTf_2]$ reveals the higher contribution of the deposition surface and the cation alkyl side chain length, rather than the anion type, for the wettability of metallic surfaces to the alkyimidazolium-based ILs. The [OTF]-series, especially those ILs constituted by long-chain alkyimidazolium cations, revealed a higher propensity for the formation of very large and more irregular 3D droplets onto ITO/glass surfaces. Both series, [OTF]-based ILs and $[NTf_2]$ -based ILs, are similar concerning their properties when the IL was deposited in the three solid surfaces studied—both presented a clear trend shift around the C_6 . The knowledge of the structural and morphological differentiations reported is truly relevant in the nanosurface science and technology of thin ionic liquid films. The different adhesion and wettability characteristics of the ILs reported here are of relevance in applications requiring a well-interface-controlled behavior of electrically conductive surfaces coated by ILs.

Supplementary Materials: The following supporting information can be downloaded at: <https://www.mdpi.com/article/10.3390/colloids6030046/s1>, Figure S1: Schematic representation of the vapor deposition methodology; Figure S2: Scheme and images of the ovens of the ThinFilmVD apparatus; Figure S3: Images of the substrate support system; Figure S4: Illustration of the mechanisms of

nucleation and growth of ionic liquid films; Figure S5: Morphology of the substrates; Figure S6: Micrographs of vapor-deposited [C₂C₁im][OTF]; Figure S7: Micrographs of vapor-deposited [C₄C₁im][OTF]; Figure S8: Micrographs of vapor-deposited [C₆C₁im][OTF]; Figure S9: Micrographs of vapor-deposited [C₈C₁im][OTF]; Figure S10: Micrographs of vapor-deposited [C₁₀C₁im][OTF]; Figure S11: Droplet size distribution of vapor-deposited ionic liquids; Figure S12: Schematic representation of the number of ionic liquid microdroplets formed and the respective surface coverage as a function of each ionic liquid in the [C_nC₁im][OTF] series; Table S1: Experimental conditions for the physical vapor deposition of each ionic liquid.

Author Contributions: Conceptualization, J.C.S.C.; methodology, M.S.M.T. and J.C.S.C.; investigation, M.S.M.T. and J.C.S.C.; writing—original draft preparation—M.S.M.T.; writing—review and editing, L.M.N.B.F.S. and J.C.S.C.; supervision, L.M.N.B.F.S. and J.C.S.C.; project administration, L.M.N.B.F.S. and J.C.S.C.; funding acquisition, L.M.N.B.F.S. All authors have read and agreed to the published version of the manuscript.

Funding: This research received no external funding.

Institutional Review Board Statement: Not applicable.

Informed Consent Statement: Not applicable.

Data Availability Statement: Not applicable.

Acknowledgments: The authors thank the Portuguese Foundation for Science and Technology (FCT) for financial support to CIQUP, Faculty of Science, University of Porto (Project UIDB/00081/2020), and IMS—Institute of Molecular Sciences (LA/P/0056/2020), Faculty of Science, University of Porto.

Conflicts of Interest: The authors declare no conflict of interest. The funders had no role in the design of the study; in the collection, analyses, or interpretation of data; in the writing of the manuscript; or in the decision to publish the results.

References

1. Hayes, R.; Warr, G.G. Structure and Nanostructure in Ionic Liquids. *Chem. Rev.* **2015**, *115*, 6357–6426. [[PubMed](#)]
2. Canongia Lopes, J.N.A.; Pádua, A.A.H. Nanostructural Organization in Ionic Liquids. *J. Phys. Chem. B* **2006**, *110*, 3330–3335. [[CrossRef](#)] [[PubMed](#)]
3. Del Pópolo, M.G.; Voth, G.A. On the Structure and Dynamics of Ionic Liquids. *J. Phys. Chem. B* **2004**, *108*, 1744–1752. [[CrossRef](#)]
4. Singh, S.K.; Savoy, A.E. Ionic Liquids Synthesis and Applications: An Overview. *J. Mol. Liq.* **2020**, *297*, 112038. [[CrossRef](#)]
5. Weingärtner, H. Understanding Ionic Liquids at the Molecular Level: Facts, Problems, and Controversies. *Angew. Chem. Int. Ed.* **2008**, *47*, 654–670. [[CrossRef](#)]
6. Sun, P.; Armstrong, D.W. Ionic Liquids in Analytical Chemistry. *Anal. Chim. Acta* **2010**, *661*, 1–16. [[CrossRef](#)]
7. Wishart, J.F.; Castner, E.W., Jr. The Physical Chemistry of Ionic Liquids. *J. Phys. Chem. B* **2007**, *111*, 4639–4640. [[CrossRef](#)]
8. Zhang, S.; Sun, N.; He, X.; Lu, X.; Zhang, X. Physical Properties of Ionic Liquids: Database and Evaluation. *J. Phys. Chem. Ref. Data* **2006**, *35*, 1475–1517. [[CrossRef](#)]
9. Werner, S.; Haumann, M.; Wasserscheid, P. Ionic Liquids in Chemical Engineering. *Annu. Rev. Chem. Biomol. Eng.* **2010**, *1*, 203–230. [[CrossRef](#)] [[PubMed](#)]
10. Gomes, J.M.; Silva, S.S.; Reis, R.L. Biocompatible Ionic Liquids: Fundamental Behaviours and Applications. *Chem. Soc. Rev.* **2019**, *48*, 4317–4335. [[CrossRef](#)]
11. Liu, H.; Yu, H. Ionic Liquids for Electrochemical Energy Storage Devices Applications. *J. Mater. Sci. Technol.* **2019**, *35*, 674–686. [[CrossRef](#)]
12. Tiago, G.A.O.; Matias, I.A.S.; Ribeiro, A.P.C.; Martins, L.M.D.R.S. Application of Ionic Liquids in Electrochemistry—Recent Advances. *Molecules* **2020**, *25*, 5812. [[CrossRef](#)] [[PubMed](#)]
13. Earle, M.J.; Esperança, J.M.S.S.; Gilea, M.A.; Canongia Lopes, J.N.; Rebelo, L.P.N.; Magee, J.W.; Seddon, K.R.; Widegren, J.A. The Distillation and Volatility of Ionic Liquids. *Nature* **2006**, *439*, 831–834. [[CrossRef](#)]
14. Esperança, J.M.S.S.; Canongia Lopes, J.N.; Tariq, M.; Santos, L.M.N.B.F.; Magee, J.W.; Rebelo, L.P.N. Volatility of Aprotic Ionic Liquids—A Review. *J. Chem. Eng. Data* **2010**, *55*, 3–12. [[CrossRef](#)]
15. Ravula, S.; Larm, N.E.; Mottaleb, M.A.; Heitz, M.P.; Baker, G.A. Vapor Pressure Mapping of Ionic Liquids and Low-Volatility Fluids Using Graded Isothermal Thermogravimetric Analysis. *ChemEngineering* **2019**, *3*, 42. [[CrossRef](#)]
16. Rocha, M.A.A.; Lima, C.F.R.A.C.; Gomes, L.R.; Schroder, B.; Coutinho, J.A.P.; Marrucho, I.M.; Esperança, J.M.S.S.; Rebelo, L.P.N.; Shimizu, K.; Canongia Lopes, J.N.; et al. High-Accuracy Vapor Pressure Data of the Extended [C_nC₁im][Ntf₂] Ionic Liquid Series: Trend Changes and Structural Shifts. *J. Phys. Chem. B* **2011**, *115*, 10919–10926. [[CrossRef](#)]

17. Almeida, H.F.D.; Freire, M.G.; Fernandes, A.M.; Lopes-da-Silva, J.A.; Morgado, P.; Shimizu, K.; Filipe, E.J.M.; Canongia Lopes, J.N.; Santos, L.M.N.B.F.; Coutinho, J.A.P. Cation Alkyl Side Chain Length and Symmetry Effects on the Surface Tension of Ionic Liquids. *Langmuir* **2014**, *30*, 6408–6418. [[CrossRef](#)]
18. Liu, H.; Jiang, L. Wettability by Ionic Liquids. *Small* **2016**, *12*, 9–15. [[CrossRef](#)] [[PubMed](#)]
19. Minea, A.A.; Murshed, S.M.S. A Review on Development of Ionic Liquid Based Nanofluids and their Heat Transfer Behavior. *Renew. Sustain. Energy Rev.* **2018**, *91*, 584–599. [[CrossRef](#)]
20. Yebra, F.; Troncoso, J.; Romani, K. Thermal Conductivity of Ionic Liquids under Pressure. *Fluid Phase Equil.* **2020**, *515*, 112573. [[CrossRef](#)]
21. Bica, K.; Deetlefs, M.; Schroder, C.; Seddon, K.R. Polarisabilities of Alkylimidazolium Ionic Liquids. *Phys. Chem. Chem. Phys.* **2013**, *15*, 2703–2711. [[CrossRef](#)] [[PubMed](#)]
22. Bhat, M.A.; Dutta, C.K.; Rather, G.M. Exploring Physicochemical Aspects of N-alkylimidazolium Based Ionic Liquids. *J. Mol. Liq.* **2013**, *181*, 142–151. [[CrossRef](#)]
23. Fadeeva, Y.A.; Gruzdev, M.S.; Kudryakova, N.O.; Shmukler, L.E.; Safonova, L.P. Physico-Chemical Characterization of Alkylimidazolium Protic Ionic Liquids. *J. Mol. Liq.* **2020**, *297*, 111305. [[CrossRef](#)]
24. Sanchora, P.; Pandey, D.K.; Kagdada, H.L.; Materny, A.; Singh, D.K. Impact of Alkyl Chain Length and Water on the Structure and Properties of 1-Alkyl-3-Methylimidazolium Chloride Ionic Liquids. *Phys. Chem. Chem. Phys.* **2020**, *22*, 17687–17704. [[CrossRef](#)]
25. Singh, T.; Kumar, A. Aggregation Behavior of Ionic Liquids in Aqueous Solutions: Effect of Alkyl Chain Length, Cations, and Anions. *J. Phys. Chem. B* **2007**, *111*, 7843–7851. [[CrossRef](#)]
26. Rocha, M.A.A.; Neves, C.M.S.S.; Freire, M.G.; Russina, O.; Triolo, A.; Coutinho, J.A.P.; Santos, L.M.N.B.F. Alkylimidazolium Based Ionic Liquids: Impact of Cation Symmetry on Their Nanoscale Structural Organization. *J. Phys. Chem. B* **2013**, *117*, 10889–10897. [[CrossRef](#)] [[PubMed](#)]
27. Zheng, W.; Mohammed, A.; Hines, L.G.; Xiao, D.; Martinez, O.J.; Bartsch, R.A.; Simon, S.L.; Russina, O.; Triolo, A.; Quitevis, E.L. Effect of Cation Symmetry on the Morphology and Physicochemical Properties of Imidazolium Ionic Liquids. *J. Phys. Chem. B* **2011**, *115*, 6572–6584. [[CrossRef](#)] [[PubMed](#)]
28. Xue, L.; Gurung, E.; Tamas, G.; Koh, Y.P.; Shadeck, M.; Simon, S.L.; Maroncelli, M.; Quitevis, E.L. Effect of Alkyl Chain Branching on Physicochemical Properties of Imidazolium-Based Ionic Liquids. *J. Chem. Eng. Data* **2016**, *61*, 1078–1091. [[CrossRef](#)]
29. Shimizu, K.; Costa Gomes, M.F.; Pádua, A.A.H.; Rebelo, L.P.N.; Canongia Lopes, J.N. Three Commentaries on the Nano-segregated Structure of Ionic Liquids. *Theochem* **2010**, *946*, 70–76. [[CrossRef](#)]
30. Abe, H.; Fukushima, R.; Onji, M.; Hirayama, K.; Kishimura, H.; Yoshimura, Y.; Ozawa, S. Two-Length Scale Description of Hydrophobic Room-Temperature Ionic Liquid–Alcohol Systems. *J. Mol. Liq.* **2016**, *215*, 417–422. [[CrossRef](#)]
31. Rodrigues, A.S.M.C.; Santos, L.M.N.B.F. Nanostructuring Effect on the Thermal Behavior of Ionic Liquids. *ChemPhysChem* **2016**, *17*, 1512–1517. [[CrossRef](#)] [[PubMed](#)]
32. Costa, J.C.S.; Alves, A.; Bastos, M.; Santos, L.M.N.B.F. The Impact of the Cation Alkyl Chain Length on the Wettability of Alkylimidazolium-Based Ionic Liquids at the Nanoscale. *Phys. Chem. Chem. Phys.* **2022**, *14*, 13343–13355. [[CrossRef](#)] [[PubMed](#)]
33. Costa, J.C.S.; Mendes, A.; Santos, L.M.N.B.F. Morphology of Imidazolium-Based Ionic Liquids as Deposited by Vapor Deposition: Micro-/Nanodroplets and Thin Films. *ChemPhysChem* **2016**, *17*, 2123–2127. [[CrossRef](#)] [[PubMed](#)]
34. Rietzler, F.; May, B.; Steinruck, H.-P.; Maier, F. Switching Adsorption and Growth behavior of Ultrathin [C₂C₁Im][OTf] films on Au(111) by Pd deposition. *Phys. Chem. Chem. Phys.* **2016**, *18*, 25143–25150. [[CrossRef](#)]
35. Costa, J.C.S.; Coelho, A.F.S.M.G.; Mendes, A.; Santos, L.M.N.B.F. Nucleation and Growth of Microdroplets of Ionic Liquids Deposited by Physical Vapor Method onto Different Surfaces. *Appl. Surf. Sci.* **2018**, *428*, 242–249. [[CrossRef](#)]
36. Campos, R.M.; Alves, A.C.P.M.; Lima, M.A.L.; Farinha, A.F.M.; Cardoso, J.P.S.; Mendes, A.; Costa, J.C.S.; Santos, L.M.N.B.F. Morphology, Structure, and Dynamics of Pentacene Thin Films and Their Nanocomposites with [C₂C₁im][NTf₂] and [C₂C₁im][OTF] Ionic Liquids. *ChemPhysChem* **2020**, *21*, 1814–1825. [[CrossRef](#)] [[PubMed](#)]
37. Maruyama, S.; Takeyama, Y.; Taniguchi, H.; Fukumoto, H.; Itoh, M.; Kumigashira, H.; Oshima, M.; Yamamoto, T.; Matsumoto, Y. Molecular Beam Deposition of Nanoscale Ionic Liquids in Ultrahigh Vacuum. *ACS Nano* **2010**, *4*, 5946–5952. [[CrossRef](#)] [[PubMed](#)]
38. Meusel, M.; Lexow, M.; Gezmis, A.; Bayer, A.; Maier, F.; Steinruck, H.-P. Growth of Multilayers of Ionic Liquids on Au(111) Investigated by Atomic Force Microscopy in Ultrahigh Vacuum. *Langmuir* **2020**, *36*, 13670–13681. [[CrossRef](#)] [[PubMed](#)]
39. Cremer, T.; Killian, M.; Gottfried, J.M.; Paape, N.; Wasserscheid, P.; Maier, F.; Steinruck, H.-P. Physical Vapor Deposition of [EMIM][Tf₂N]: A New Approach to the Modification of Surface Properties with Ultrathin Ionic Liquid Films. *ChemPhysChem* **2008**, *9*, 2185–2190. [[CrossRef](#)]
40. Borghi, F.; Podestà, A. Ionic Liquids under Nanoscale Confinement. *Adv. Phys. X* **2020**, *5*, 1736949. [[CrossRef](#)]
41. Richey, N.E.; Paula, C.; Bent, S.F. Understanding Chemical and Physical Mechanisms in Atomic Layer Deposition. *J. Chem. Phys.* **2020**, *152*, 040902. [[CrossRef](#)]
42. Venables, J.A.; Spiller, G.D.T.; Hanbucken, M. Nucleation and Growth of Thin Films. *Rep. Progr. Phys.* **1984**, *47*, 399–459. [[CrossRef](#)]
43. Venables, J.A.; Spiller, G.D.T. Nucleation and Growth of Thin Films. In *Surface Mobilities on Solid Materials*; Springer: Boston, MA, USA, 1983; pp. 341–404.
44. Ratsch, C.; Venables, J.A. Nucleation Theory and the Early Stages of Thin Film Growth. *J. Vac. Sci. Technol. A Vacuum Surfaces Films* **2003**, *21*, S96–S109. [[CrossRef](#)]

45. Young, T. An Essay on the Cohesion of Fluids. *Philos. Trans. R. Soc. Lond.* **1805**, *95*, 65–87.
46. Adam, N.K. Use of the Term ‘Young’s Equation’ for Contact Angles. *Nature* **1957**, *180*, 809–810. [[CrossRef](#)]
47. Wenzel, R.N. Surface Roughness and Contact Angle. *J. Phys. Chem.* **1949**, *53*, 1466–1467. [[CrossRef](#)]
48. Giljean, S.; Bigerelle, M.; Anselme, K.; Haidara, H. New Insights on Contact Angle/Roughness Dependence on High Surface Energy Materials. *Appl. Surf. Sci.* **2011**, *257*, 9631–9638. [[CrossRef](#)]
49. Foadi, F.; Vaez Allaei, S.M.; Palasantzas, G.; Mohammadzadeh, M.R. Roughness-Dependent Wetting Behavior of Vapor-Deposited Metallic Thin Films. *Phys. Rev. E* **2019**, *100*, 022804. [[CrossRef](#)]
50. Weijss, J.H.; Marchand, A.; Andreotti, B.; Lohse, D.; Snoeijer, J.H. Origin of Line Tension for a Lennard-Jones Nanodroplet. *Phys. Fluids* **2011**, *23*, 022001. [[CrossRef](#)]
51. Zhang, J.; Wang, P.; Borg, M.K.; Reese, J.M.; Wen, D. A Critical Assessment of the Line Tension Determined by the Modified Young’s Equation. *Phys. Fluids* **2018**, *30*, 082003. [[CrossRef](#)]
52. Deyko, A.; Cremer, T.; Rietzler, F.; Perkin, S.; Crowhurst, L.; Welton, T.; Steinruck, H.-P.; Maier, F. Interfacial Behavior of Thin Ionic Liquid Films on Mica. *J. Phys. Chem. C* **2013**, *117*, 5101–5111. [[CrossRef](#)]
53. Costa, J.C.S.; Rocha, R.M.; Vaz, I.C.M.; Torres, M.C.; Mendes, A.; Santos, L.M.N.B.F. Description and Test of a New Multilayer Thin Film Vapor Deposition Apparatus for Organic Semiconductor Materials. *J. Chem. Eng. Data* **2015**, *60*, 3776–3791. [[CrossRef](#)]
54. Costa, J.C.S.; Azevedo, J.; Araújo, J.P.; Santos, L.M.N.B.F.; Mendes, A. High Purity and Crystalline Thin Films of Methylammonium Lead Iodide Perovskites by a Vapor Deposition Approach. *Thin Solid Films* **2018**, *664*, 12–18. [[CrossRef](#)]
55. Costa, J.C.S.; Mendes, A.; Santos, L.M.N.B.F. Thin Film Deposition of Organic Hole Transporting Materials: Optical, Thermodynamic and Morphological Properties of Naphthyl-Substituted Benzidines. *J. Mater. Sci.* **2018**, *53*, 12974–12987. [[CrossRef](#)]
56. Santos, L.M.N.B.F.; Lobo Ferreira, A.I.M.C.; Štefja, V.; Rodrigues, A.S.M.C.; Rocha, M.A.A.; Torres, M.C.; Tavares, F.M.S.; Carpinteiro, F.S. Development of the Knudsen Effusion Methodology for Vapour Pressure Measurements of Low Volatile Liquids and Solids Based on a Quartz Crystal Microbalance. *J. Chem. Thermodyn.* **2018**, *126*, 171–186. [[CrossRef](#)]
57. Swift, P. Adventitious Carbon—The Panacea for Energy Referencing? *Surf. Interface Anal.* **1982**, *4*, 47–51. [[CrossRef](#)]
58. Schneider, C.A.; Rasband, W.S.; Eliceiri, K.W. NIH Image to ImageJ: 25 Years of Image Analysis. *Nat. Methods* **2012**, *9*, 671–675. [[CrossRef](#)] [[PubMed](#)]
59. Foulston, R.; Gangopadhyay, S.; Chiutu, C.; Moriarty, P.; Jones, R.C. Mono- and Multilayer Adsorption of an Ionic Liquid on Au(110). *Phys. Chem. Chem. Phys.* **2012**, *14*, 6054–6066. [[CrossRef](#)]
60. Uhl, B.; Huang, H.; Alwast, D.; Buchner, F.; Behm, R.J. Interaction of Ionic Liquids with Noble Metal Surfaces: Structure Formation and Stability of [OMIM][TFSA] and [EMIM][TFSA] on Au(111) and Ag(111). *Phys. Chem. Chem. Phys.* **2015**, *17*, 23816–23832. [[CrossRef](#)] [[PubMed](#)]
61. Pereira, M.M.; Kurnia, K.A.; Sousa, F.L.; Silva, N.J.O.; Lopes da Silva, J.A.; Coutinho, J.A.P.; Freire, M.G. Contact Angles and Wettability of Ionic Liquids on Polar and non-Polar Surfaces. *Phys. Chem. Chem. Phys.* **2015**, *17*, 31653–31661. [[CrossRef](#)] [[PubMed](#)]
62. Delcheva, I.; Beattie, D.A.; Ralston, J.; Krasowska, M. Dynamic Wetting of Imidazolium-Based Ionic Liquids on Gold and Glass. *Phys. Chem. Chem. Phys.* **2018**, *20*, 2084–2093. [[CrossRef](#)] [[PubMed](#)]
63. Delcheva, I.; Ralston, J.; Beattie, D.A.; Krasowska, M. Static and Dynamic Wetting Behaviour of Ionic Liquids. *Adv. Colloid Interface Sci.* **2015**, *222*, 162–171. [[CrossRef](#)] [[PubMed](#)]
64. Carrera, G.V.S.M.; Afonso, C.A.M.; Branco, L.C. Interfacial Properties, Densities, and Contact Angles of Task Specific Ionic Liquids. *J. Chem. Eng. Data* **2010**, *55*, 609–615. [[CrossRef](#)]
65. Lexow, M.; Maier, F.; Steinruck, H.-P. Ultrathin Ionic Liquid Films on Metal Surfaces: Adsorption, Growth, Stability and Exchange Phenomena. *Adv. Phys. X* **2020**, *5*, 1761266. [[CrossRef](#)]
66. Lexow, M.; Talwar, T.; Heller, B.S.-J.; May, B.; Bhuin, R.G.; Maier, F.; Steinruck, H.-P. Time-Dependent Changes in the Growth of Ultrathin Ionic Liquid Films on Ag(111). *Phys. Chem. Chem. Phys.* **2018**, *20*, 12929–12938. [[CrossRef](#)]
67. Cremer, T.; Stark, M.; Deyko, A.; Steinruck, H.-P.; Maier, F. Liquid/Solid Interface of Ultrathin Ionic Liquid Films: [C₁C₁Im][Tf₂N] and [C₈C₁Im][Tf₂N] on Au(111). *Langmuir* **2011**, *27*, 3662–3671. [[CrossRef](#)]
68. Meusel, M.; Lexow, M.; Gezmis, A.; Schötz, S.; Wagner, M.; Bayer, A.; Maier, F.; Steinruck, H.-P. Atomic Force and Scanning Tunneling Microscopy of Ordered Ionic Liquid Wetting Layers from 110 K up to Room Temperature. *ACS Nano* **2020**, *14*, 9000–9010. [[CrossRef](#)]
69. Jha, K.C.; Liu, H.; Bockstaller, M.R.; Heinz, H. Facet Recognition and Molecular Ordering of Ionic Liquids on Metal Surfaces. *J. Phys. Chem. C* **2013**, *117*, 25969–25981. [[CrossRef](#)]
70. Atkin, R.; El Abedin, S.Z.; Hayes, R.; Gasparotto, L.H.S.; Borisenko, N.; Endres, F. AFM and STM Studies on the Surface Interaction of [BMP]TFSA and [EMIm]TFSA Ionic Liquids with Au(111). *J. Phys. Chem. C* **2009**, *113*, 13266–13272. [[CrossRef](#)]
71. Kamalakannan, S.; Prakash, M.; Chambaud, G.; Hochlaf, M. Adsorption of Hydrophobic and Hydrophilic Ionic Liquids at the Au(111) Surface. *ACS Omega* **2018**, *3*, 18039–18051. [[CrossRef](#)] [[PubMed](#)]
72. Borghi, F.; Mirigliano, M.; Lenardi, C.; Milani, P.; Podestà, A. Nanostructure Determines the Wettability of Gold Surfaces by Ionic Liquid Ultrathin Films. *Front. Chem.* **2021**, *9*, 619432. [[PubMed](#)]
73. Hessey, S.G.; Jones, R.G. On the Evaporation, Bonding, and Adsorbate Capture of an Ionic Liquid on Au(111). *Chem. Sci.* **2013**, *4*, 2519–2529.